REPORT DOCUMENTATION PAGE

AD-A200 679 DTIC ELECTE S JUL 13 1988 D CY

1b. RESTRICTIVE MARKINGS	
2b. DECLASSIFICATION / DOWNGRADING SCHEDULE	3. DISTRIBUTION / AVAILABILITY OF REPORT: Approved for public release; distribution is unlimited.
4. PERFORMING ORGANIZATION REPORT NUMBER(S)	5. MONITORING ORGANIZATION REPORT NUMBER(S): AFOSR-TR- 88-1089
6a. NAME OF PERFORMING ORGANIZATION: Stanford University	6b. OFFICE SYMBOL (If applicable):
6c. ADDRESS (City, State, and ZIP Code): 660 Arguello Way, Encina Hall, Stanford, CA 94305-6060	7a. NAME OF MONITORING ORGANIZATION: AFOSR/NP
	7b. ADDRESS (City, State, and ZIP Code): Building 410, Bolling AFB DC 20332-6448
8a. NAME OF FUNDING / SPONSORING ORGANIZATION: AFOSR	8b. OFFICE SYMBOL (If applicable): NP
	9. PROCUREMENT INSTRUMENT IDENTIFICATION NUMBER: F49620-85-C-0062
8c. ADDRESS (City, State, and ZIP Code): Building 410, Bolling AFB DC 20332-6448	10. SOURCE OF FUNDING NUMBERS: PROGRAM ELEMENT NO. 61102F; PROJECT NO. 2301; TASK NO. A1; WORK UNIT ACCESSION NO.

11. TITLE (Include Security Classification)

(U) LASER PHYSICS AND LASER SPECTROSCOPY

12. PERSONAL AUTHOR(S)

Dr Robert L. Byer

13a. TYPE OF REPORT	13b. TIME COVERED	14. DATE OF REPORT (Year, Month, Day)	15. PAGE COUNT
FINAL	FROM 1 Mar 85 TO 29 Feb 88		21

16. SUPPLEMENTARY NOTATION

17. COSATI CODES			18. SUBJECT TERMS (Continue on reverse if necessary and identify by block number)
FIELD	GROUP	SUB-GROUP	
	20.06		

19. ABSTRACT (Continue on reverse if necessary and identify by block number)

The research proposal for this program emphasized the production of single-crystal fiber optical devices. We report results in the growth, processing, and characterization of single-crystal fibers, which have led to significant demonstrations of fiber laser and nonlinear optical devices. Theoretical work originally undertaked to model fiber materials and device behavior has contributed to the development of the more general concept of tailored nonlinear media. This concept, and the materials work toward understanding fiber device processing, resulted in the development of new non-linear materials, through the modification of existing materials or through microscopic control of material structure during growth.

20. DISTRIBUTION / AVAILABILITY OF ABSTRACT	21. ABSTRACT SECURITY CLASSIFICATION
☒ UNCLASSIFIED/UNLIMITED ☒ SAME AS RPT. ☐ DTIC USERS	UNCLASSIFIED
22a. NAME OF RESPONSIBLE INDIVIDUAL: H R Schlossberg	22b. TELEPHONE (Include Area Code): 202/767-4906 — 22c. OFFICE SYMBOL: AFOSR/NP

DD FORM 1473, 84 MAR 83 APR edition may be used until exhausted. All other editions are obsolete.

SECURITY CLASSIFICATION OF THIS PAGE

UNCLASSIFIED

88 1011 123

Edward L. Ginzton Laboratory
Stanford University
Stanford, California 94305

LASER PHYSICS AND LASER SPECTROSCOPY

Final Technical Report

for

Air Force Office of Scientific Research

Contract number: F49620-85-C-0062

for the period

March 1, 1985 to February 29, 1988

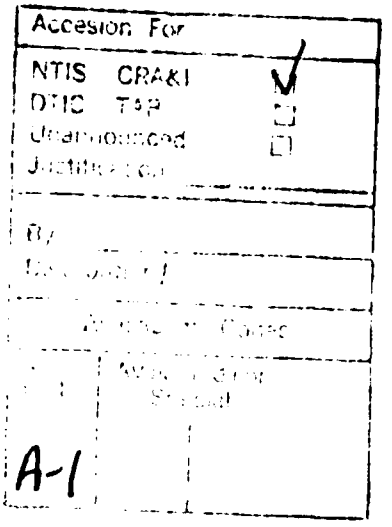

GL Report No. _____

Principal Investigator:

Robert L. Byer

Applied Physics Department
Stanford University
(415) 723-0226

March, 1988

LASER PHYSICS AND LASER SPECTROSCOPY

Final Technical Report
March, 1988

ABSTRACT

The research proposal for this program emphasized the production of single-crystal fiber optical devices. We report results in the growth, processing, and characterization of single-crystal fibers, which have led to significant demonstrations of fiber laser and nonlinear optical devices. Theoretical work originally undertaken to model fiber materials and device behavior has contributed to the development of the more general concept of tailored nonlinear media. This concept, and the materials work toward understanding fiber device processing, resulted in the development of new nonlinear optical materials, through the modification of existing materials or through the microscopic control of material structure during growth.

Specifically, single-crystal fibers with rms diameter stability of better than 0.07% were grown. Sapphire fibers nearly a meter long were grown which should exhibit total losses on the order of 0.1 dB/m at the useful wavelength of 2.9 μm. Methods for cladding $LiNbO_3$ fibers were studied, resulting in the propagation of a 14-μm diameter fundamental mode in a magnesium-indiffused fiber. A model explaining the ferroelectric domain structures of $LiNbO_3$ fibers was applied to the modification of the domain structures in fibers and in $LiNbO_3$ slabs. Characterization techniques were developed for measuring the refractive index profiles and scattering losses in single-crystal fibers. Monolithic fiber lasers were demonstrated, as was guided-wave second harmonic generation in a clad $LiNbO_3$ fiber. New Cr-doped oxide laser materials were studied. A vapor transport equilibration process was used to change the composition of $LiNbO_3$ enough to allow the noncritically phasematched second harmonic generation of 477-nm light, the shortest wavelength produced in a bulk interaction in this material. Photochemical changes in the structure and optical properties of polysilane films, causing a large third-order nonlinear effect, were discovered. Finally, by applying DC electric fields to AlGaAs quantum well material, second-order nonlinearities larger than those reported for any other material were induced.

LASER PHYSICS AND LASER SPECTROSCOPY

Final Technical Report
March, 1988

TABLE OF CONTENTS

I. Introduction and Objectives 1

II. Summary of Major Accomplishments 3

A. Single-Crystal Fiber Devices 3

B. Theoretical Work 5

C. Development of New Materials 6

III. Progress and Accomplishments in the Past Year 8

A. Single-Crystal Fibers and Lithium Niobate 8

B. Second Harmonic Generation in DC-Biased Quantum Wells 21

C. Structural and Optical Studies of Thin Polysilane Films 26

IV. Proposed Future Research Directions 32

A. Oxide Crystals 32

B. SHG in DC-Biased Quantum Wells 33

C. Nonlinear Optical Properties of Polysilane Films 34

V. Collaborations 35

VI. Publications, Presentations, and Patents 36

VII. Personnel Associated with the Program 39

LASER PHYSICS AND LASER SPECTROSCOPY

Final Technical Report
March, 1988

I. INTRODUCTION AND OBJECTIVES

The development of single-crystal optical fibers makes possible devices which would either be impossible in glass fibers because of their amorphous structure, or which would take excessive lengths of glass fiber to implement. Crystal fibers possess a geometry naturally suited for coupling to glass fibers now widely used in data-communication systems. Examples of possible devices can be divided into three qualitatively different classes. The passive class of devices includes lightguides, polarizers, isolators, and filters. Active devices are represented by fiber lasers and amplifiers. Finally, nonlinear devices, which take advantage of the sustained high field intensities achievable in fiber waveguides to dramatically increase the efficiency of nonlinear interactions, include harmonic generators, Raman shifters, and optical parametric oscillators.

This research program has concentrated upon single-crystal fiber materials which are applicable to all three classes of devices. Single-crystal sapphire (Al_2O_3) is transparent over at least the 0.24 – 4.0 μm wavelength range, is birefringent, and possesses a high melting point, making it useful for passive devices such as polarizers, filters, and high-temperature lightguides. Because of the ease with which it can be grown, it has also been a good crystal to use in studying the single-crystal fiber growth process. Ruby ($Cr:Al_2O_3$), Nd:YAG, and other oxides doped with chromium can be used to make active devices. Lithium niobate ($LiNbO_3$) has been studied for application to nonlinear devices. Magnesium doping has been shown to lessen the effects of photorefractive damage in $LiNbO_3$, and hence the magnesium-doped material is most often grown.

The main objectives of this program have been the growth, fabrication, and characterization of various single-crystal fiber materials and devices. Growth process development has as its goals the production of fibers with stable (or intentionally

modulated) diameter and constant (or controlled varied) composition. Fiber fabrication includes all post-growth steps in the making of devices, such as end polishing, and annealing for improving mechanical strength and compositional uniformity. Also studied are stoichiometry control via diffusion, poling of ferroelectric fibers to make them single-domain (or some other desirable domain structure), and formation of diffused or coated claddings to protect the guiding interface or to reduce its diameter. Finally, characterization of the resulting fiber device at several points during fabrication is necessary to determine the success of the various processing steps and, after the device is completed, to measure its operating parameters and performance.

An essential part of the device development effort has been the investigation of the control and modification of materials used in optical devices. Indeed, materials studies have comprised a major portion of the research effort under this program. A realization of the wide control of materials properties which is possible during and after materials growth has led to a broader vision of the engineering of "synthetic nonlinear media." Our research now extends past the study of single-crystal fibers to the design and optical characterization of novel III-V semiconductor structures and organic nonlinear materials, fields in which we have already made significant advances since we began our work on them just a year ago.

II. SUMMARY OF MAJOR ACCOMPLISHMENTS

The research proposal for this program emphasized the production of single-crystal fiber optical devices. We are able to report impressive results in the growth, processing, and characterization of single-crystal fibers, which have led to significant demonstrations of fiber laser and nonlinear optical devices. Theoretical work originally undertaken to model fiber materials and device behavior has contributed to the development of the more general concept of tailored nonlinear media. This concept, and the materials work toward understanding fiber device processing, have resulted in the development of new laser and nonlinear optical materials, through the modification of existing materials or through the microscopic control of material structure during growth.

A. Single-Crystal Fiber Devices

1. Fiber crystal growth

Single-crystal sapphire fibers are used to tune up the performance of the growth machine. As a result, the growth of sapphire fibers is the best-characterized and best-developed of all the materials studied. The crystal quality and chemical inertness of sapphire fibers 150 μm in diameter were well demonstrated by a bending test in which the fiber broke after being pulled into a loop of ~ 5 mm diameter, corresponding to a maximum strain of 3%, approaching the theoretical cohesive strength of solid matter. Intentional diameter modulation was demonstrated with a period of ~ 5 μm for a 3 Hz modulation of the pull rate. The maximum growth rate in air before the onset of the formation of bulk microvoids in sapphire fibers was determined to be ~ 10 mm/min, well above the usual growth rate of 1–2 mm/min. Sapphire fibers **nearly a meter** long have been grown, a length which should be adequate for many important applications.

The stabilization of heating laser power and the installation of a computer feedback control loop to correct motor speeds during growth led to the closed-loop growth of sapphire and $LiNbO_3$ fibers with rms diameter stability of **less than 0.07%**. This level of diameter control is adequate for even the most critical nonlinear applications. The diameter monitoring equipment has also enabled the measurement of growth process transfer functions, which allows us to test the validity of theoretical models of the fiber growth process, and eventually to design even more effective diameter controllers.

2. Fiber processing

Several techniques for cladding $LiNbO_3$ fibers were studied. It was possible to guide low-order modes of one polarization in a fiber clad using proton exchange. This process changes only one index of refraction (n_o) in the proper direction for cladding (downward), so an alternative method was sought for nonlinear fiber devices. Tantalum indiffusion was found to have a very low diffusion coefficient and to adversely affect the ferroelectric domain structure of fibers. The solution was found to be magnesium indiffusion. Using this process, it was possible to propagate a **14-μm diameter fundamental mode** in a 3-mm long, 56-μm diameter *c*-axis fiber. Electron microprobe analysis conducted during the course of Mg cladding characterization experiments also led to the discovery of the formation of a magnesium-rich intermediate compound which affects the cladding process. This kind of knowledge gained about magnesium diffusion may also be of use to researchers using this technology to form buried integrated-optic waveguides.

The ferroelectric domain structures of as-grown $LiNbO_3$ fibers were studied, and a model for their unusual configuration was proposed. This model suggested methods for altering the domain structure during or after growth. Successful growth of fibers with domain walls offset from the center of the fiber, and with periodically alternating domains with a period on the order of 10 μm were subsequently achieved.

Polishing techniques producing perpendicular end faces for fiber resonators were developed. Simpler procedures for the polishing of non-resonator devices were also successfully applied to fibers of sapphire and $LiNbO_3$. Apparatus facilitating the handling of extremely delicate 50-μm $LiNbO_3$ device fibers was also developed.

3. Characterization

An integrating sphere technique for the measurement of the scattering losses of fibers was developed, and used to infer total losses in sapphire fibers as low as **0.08 dB/m** at useful wavelengths in the mid-infrared.

Two techniques for the measurement of refractive index profiles in crystal fibers were developed and applied to diffusion-clad $LiNbO_3$ fibers and glass-clad Nd:YAG laser fibers. The first method, an adaptation of reflectometry to use polarized probe light, proved most useful for refractive index steps due to its sensitivity to the condition of the fiber

surface. A magnifying form of a Mach-Zehnder interferometer was used to determine the graded index profiles due to Mg indiffusion.

4. Device demonstrations

Work on monolithic resonator fiber lasers, in which the mirrors are coated directly onto the polished fiber endfaces, was extended to the production of a dielectric-coated Nd:YAG fiber laser. This laser operated with a threshold of only 3.7 mW, and a slope efficiency of greater than 10%. More than 80% of the laser power was in the fundamental spatial mode. The efficiency of fiber lasers was due to the polishing technology, which ensured the perpendicularity of the mirror faces, and to fiber diameter control, which minimized scattering losses along the fiber.

Guided-wave second harmonic generation in a clad $LiNbO_3$ fiber was demonstrated for the first time. The observed low efficiency can be attributed to the multimode propagation properties of the fiber. A factor of ~ 50 enhancement over the efficiency of an optimally-focused bulk interaction in the same length sample is expected upon the development of better-controlled diffused claddings.

B. Theoretical Work

As mentioned earlier, a thermoelectric model was found to explain the domain structure of as-grown $LiNbO_3$ fibers. This model may also explain domain inversion effects which have been observed in the fabrication of integrated optic devices. The thermoelectric effect can perhaps be used in conjunction with selective lithium outdiffusion, which lowers the ferroelectric transition temperature where Li has been lost, to fabricate periodically-poled structures on $LiNbO_3$ slab surfaces for use in quasi-phasematching nonlinear interactions in an integrated optic waveguide.

A theory for mode propagation and radiation losses in anisotropic dielectric waveguides with arbitrary orientation of the axes of the dielectric tensor was developed. It has application to angle-tuned waveguide nonlinear optical devices.

The second-order nonlinear susceptibility due to intersubband transitions in AlGaAs quantum wells biased by an applied electric field has been modeled. Numerical calculations based on this theoretical model were used in the interpretation of experimental data which show a susceptibility over two orders of magnitude larger than that of bulk GaAs.

C. Development of New Materials

The fiber growth process is rapid compared to the growth of larger bulk crystals, making it useful in materials surveys. For example, new materials for tunable lasers were grown in fiber form to investigate the influence of the host on the fluorescence wavelength. The materials were Cr-doped scandium oxide, yttrium oxide, lutetium oxide, and mixtures of scandium oxide with the two other compounds. The preliminary measurements on lifetime and intensity of the fluorescence indicated that tunable solid-state lasers emitting in the near-infrared will be a reality.

The Vapor Transport Equilibration (VTE) process to exchange lithium between a source of constant activity and a test sample was originally used by Holman and co-workers to study the phase diagram of $LiNbO_3$. We originally suggested the use of VTE in the course of our $LiNbO_3$ fiber work as a means of controlling the composition of as-grown fibers to be that of the source material. This ensures that the composition is both homogeneous and well-known for keeping conditions similar for further processing experiments. We soon realized, however, that by using this technique we could attain compositions that cannot be obtained from crystal growth, and within reasonable times for small samples. This raised the possibility of altering the birefringence of the material for control of the phasematching properties. The result of these investigations was the creation of truly stoichiometric $LiNbO_3$, in which the phasematching temperature for frequency doubling 1.06-μm light was raised to 238°C. This increase in the birefringence allowed the noncritically phasematched **second harmonic generation of 477-nm radiation, the shortest wavelength ever produced in a bulk interaction in $LiNbO_3$.**

In our recently-initiated investigation of the polysilane class of organic nonlinear materials, we discovered photochemical changes of the structure and concomitant changes in the optical properties of polysilane films. A very large third-order nonlinearity due to this process can be inferred. It may be possible to use this effect to fabricate channel waveguides in the films through photoexposure. We could thereby gain the advantages of waveguide optical confinement to further enhance the efficiency of $\chi^{(3)}$ interactions such as might be useful in all-optical computing.

The general concept of synthetic nonlinear media is perhaps best exemplified in the control of the structure of a medium on a microscopic scale represented by the growth of quantum-well structures in AlGaAs. By biasing quantum-well material with a DC field, second-order nonlinearities a factor of 300 larger than that of bulk GaAs were induced (the

largest $d^{2\omega}$ reported for any material), enabling second harmonic generation using intersubband transitions. The controllability of the sign and magnitude of the nonlinearity using applied fields make quasi-phasematching feasible in this structure as well, providing yet another degree of freedom in the engineering of this synthetic nonlinear medium.

III. PROGRESS AND ACCOMPLISHMENTS IN THE PAST YEAR

A. Single-Crystal Fibers and Lithium Niobate

1. Fiber growth

Diameter control. Careful empirical tuning of the digital diameter controller has resulted in the smoothest sapphire and $LiNbO_3$ fibers ever produced. The best 170-μm $LiNbO_3$ fiber exhibits a peak-to-peak diameter variation of only about 0.3 μm, corresponding to an rms fluctuation of 0.07% or better, over its entire length of several centimeters. This level of diameter control is entirely adequate for nonlinear device purposes. A section of the diameter-vs-length plot taken while this fiber was growing is shown in Fig. 1. (The smoothest sapphire fiber has comparable peak-to-peak diameter fluctuations, but because of the better-damped control loop tuning that is possible with the different material, possesses much less of the high-spatial-frequency periodic noise which is apparent in Fig. 1.)

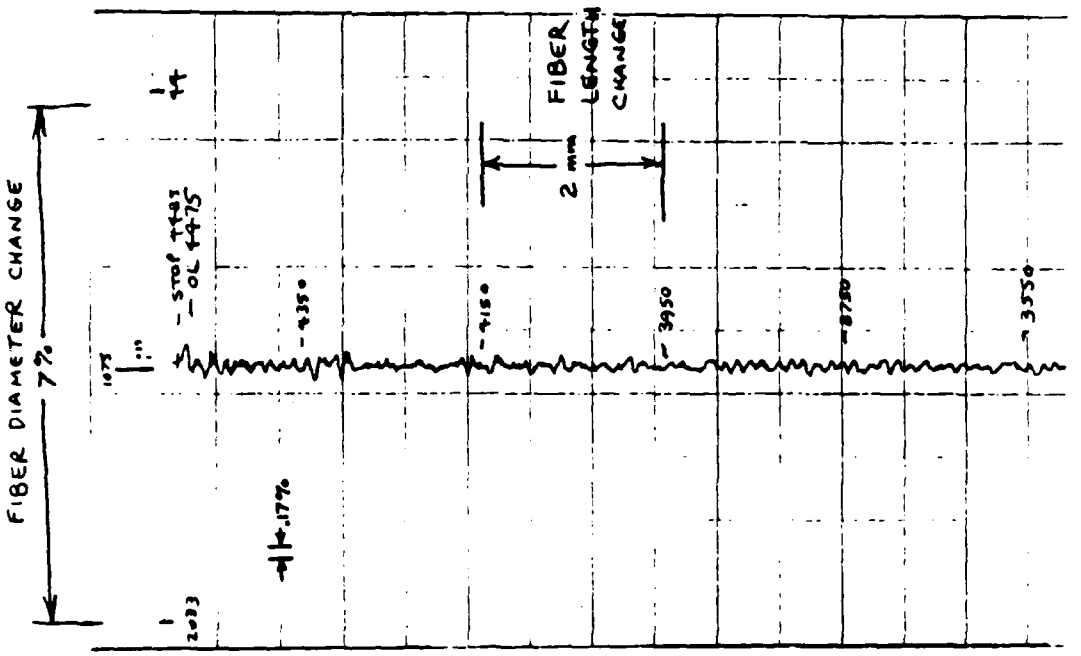

Fig. 1. Plot of diameter vs length for 170-μm diameter fiber N-324. Careful tuning of the computer diameter controller resulted in an rms diameter stability of better than 0.07%.

Transfer function measurements. In order to test the validity of our theoretical model for the dynamics of fiber growth, and to help develop more sophisticated diameter controllers, transfer function measurements are necessary. As an example, the feed rate at which the source material is supplied to the molten zone can be varied, and the resulting change in diameter monitored and stored in a computer using the same apparatus already developed for diameter control. The major difficulty lies in the strong dependence of the diameter on the intensity of the heating laser. Even though the stabilized laser has a long term drift in output power of only 0.2%, the resultant diameter variation can be on the order of 10 – 30%. This is much larger than the signal to be detected from the feed rate modulation. To overcome this problem, the diameter is recorded over many periods of a sinusoidal modulation. Since the period of the expected signal is known, it is possible to obtain a good estimate of the the diameter-change amplitude at this period.

The data collected up to this time are preliminary and not fully analyzed, but some results can be presented. In Fig. 2, the resulting diameter change is shown as a function of the modulation period. The fibers were grown from sapphire rods 400 μm in diameter. The two curves are for different diameter reduction ratios as labeled. At short periods, the amplitude of the signal decreases as expected. The theory predicts a second-order system with a high frequency roll-off of slope –2 on a logarithmic scale. The observed slope with increasing modulation frequency is –1.5. This discrepancy seems to be caused by thermal effects and is under investigation. The signal levels for the higher reduction ratio are generally higher which means that the growth is less stable and a perturbation in the feed rate will have a dramatic effect on the diameter. This observation is in agreement with the theory.

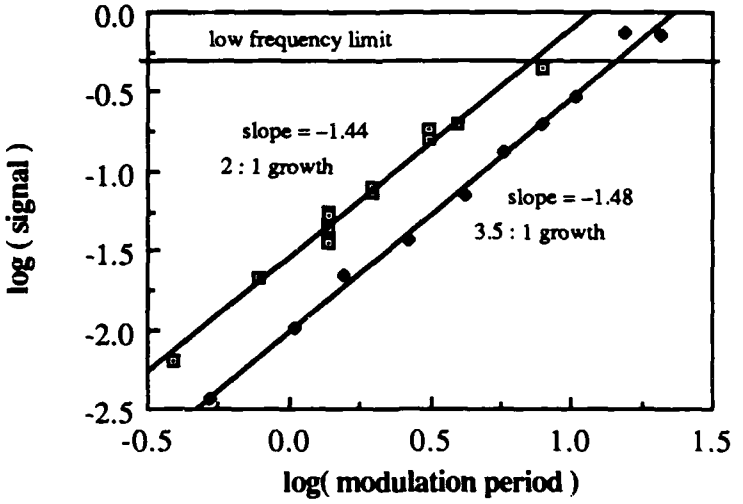

Fig. 2. Diameter variation of sapphire fibers resulting from a modulation in the feed rate during growth.

Growth of long sapphire fibers for high temperature and medical applications. For many practical applications, it is desirable to be able to grow sapphire fibers with lengths on the order of 1 m. That length allows the guiding of light out of a very hot environment such as a combustion chamber where it easily can be coupled into a conventional glass fiber. It also provides flexibility for surgical applications, in which sapphire fibers' low loss around 3 μm is of particular interest for the transmission of Er:YAG laser radiation with a wavelength of 2.9 μm.

We have grown the first fibers with the desired length and a diameter of 130 μm. The first step for characterization of these long fibers is to measure the scattering loss due to diameter variations. The technique used has been described elsewhere (see Publication No. 11), and involves collecting the scattered light with an integrating sphere. We found that a clean fiber surface is of great importance. In practical applications where low loss is important, a jacket will be necessary. The loss coefficients measured are comparable to the ones measured on shorter fibers. Two measurements are shown in Fig. 3 on a 0.77-m long fiber. The much larger scattering loss of one of the measurements is due to dirt (such as finger grease) on the surface of the fiber. The expected loss at 2.9 μm is lower so that less than 3% of the launched light should be lost in a 1-m long fiber. Measurements at other

wavelengths are under way. We also plan to measure the maximum peak and average optical power that such a fiber can guide without damage.

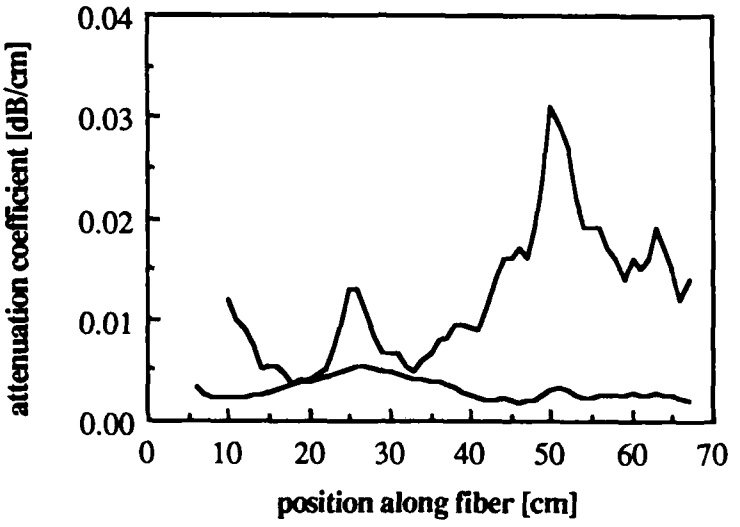

Fig. 3. The attenuation coefficient measured along a 0.77-m long sapphire fiber. The higher loss curve was measured when the fiber surface had not been cleaned.

$LiNbO_3$ fibers for nonlinear optical applications. The growth of final device size fibers around 50 μm in diameter is still difficult. Part of the difficulty lies in maintaining alignment of the heating laser with the tip of the small-diameter source fiber as growth progresses. Procedures for source rod alignment have been developed which greatly improve the straightness of the source. Another difficulty lies in diameter measurement; the smaller fibers scatter less light to the detector array which looks at the interference fringes, and positioning of the diameter probe beam is more critical. These effects may be alleviated by the installation of a new probe beam focusing lens which has recently been received.

Surface defects have been noticed to appear on $LiNbO_3$ fibers during growth. Experiments indicate that they are probably Li_2O which evaporates from the molten zone and recondenses as crystallites on the fiber at a sufficient distance from the heat source. We have found that these crystallites can be readily dissolved by immersing the fiber for a few minutes in boiling water. Further subtle ripples on the fiber surface can be seen after this treatment; these features disappear upon heating to high temperatures, either during poling experiments in the fiber grower using laser heating, or after an 1150°C anneal in a tube furnace. This indicates that whether these ripples would affect a cladding diffusion or not,

they can be removed in the normal series of processing steps, either at the poling or annealing stage.

2. Poling

Fibers — laser heating. A thermoelectric model for the self-poling of fibers during growth (see Publication No. 8) successfully explains the as-grown ferroelectric domain structure. It should also be possible to pole single-crystal $LiNbO_3$ fibers after growth by applying temperature gradients near the Curie temperature. We have conducted initial experiments on altering the domain structure of fibers after growth by the application of very large temperature gradients using laser heating in the fiber growth apparatus.

We first developed a technique for side-polishing and etching the *y* face of 170-μm fibers in order to reveal the domain structure along the entire length of the sample. This permitted the investigation of several experimental conditions on each polished and etched sample. Then both undoped and MgO-doped $LiNbO_3$ fiber samples were heated asymmetrically to the point of glowing and almost melting in the fiber grower. The heating pattern was controlled by the use of masks in the CO_2 focusing optics within the growth chamber. The *c*-axis fibers, which grow with a single domain oriented along the fiber axis, were heated to melting at the tip to gauge the melting threshold, and then heated in rings spaced widely compared to the expected temperature decay lengths along the length of the fiber. The *a*-axis fibers, which grow naturally with two domains pointing outward from a central axial domain wall, were heated from one *c* face. Both wet oxygen and helium atmospheres were used; the helium heat transfer properties should have resulted in larger applied thermal gradients within those fibers. In no case were there signs of counter-poling due to the applied gradients. For the case of the *a*-axis fibers, this may be the result of the Curie isotherm lying in a region which is already poled in the direction being encouraged by the applied gradient. No explanation has been found for the "stubborn" behavior of the *c*-axis fibers. It may be necessary to increase the background temperature of the fiber to nearer the Curie point so that smaller gradients and better position control of the Curie isotherm can be used.

Slabs. Earlier this year, Nakamura *et al.* [Appl. Phys. Lett. **50**, 1413 (1987)] reported that ferroelectric domain inversion can occur in thin lithium niobate plates that undergo heat treatment at a temperature below the Curie temperature, and then are quickly cooled. They found that the thickness of the inversion layer depended on the conditions of

the heat treatment, and postulated a pyroelectric mechanism along with lithium outdiffusion as the cause of the domain inversion. However, the polarity of the domains is consistent with the explanation that thermoelectric fields, as described by Luh *et al.* in Publication No. 8, are responsible for the domain inversion. We have conducted experiments to demonstrate this, and are submitting a paper containing our results to Applied Physics Letters.

These experiments consisted of soaking 0.5-mm thick slab samples at a high temperature below the Curie temperature either with or without the presence of $LiNbO_3$ powder, and then cooling the samples with an initial cooling rate of 50°C per minute. Without the powder, we have reproduced the results of Nakamura *et al.* Using powder, we have shown that suppressing Li_2O out-diffusion prevents surface domain inversion at 1110°C. Starting with a random domain distribution in the slab, we still end up with two antiparallel domains. This result argues against a pyroelectric interpretation, which would seem to require initially uniform domains (since the pyroelectric coefficient changes sign with the spontaneous polarization), and in favor of the thermoelectric hypothesis, which needs no such restriction on the initial conditions.

We are working on extending this technique to the use of selective Li out-diffusion for periodic poling in planar geometries. This achievement would allow quasi-phasematching to be used in nonlinear integrated optic devices.

Fibers — furnace heating. The slab poling work suggested trying the same rapid cooling technique on $LiNbO_3$ fibers. If the thermoelectric fields caused the same type of "counter-poling" in fibers that was observed in slabs, the initially outward-pointing domains in the as-grown fibers would be reversed, at least at the *c* surfaces of the fibers, to inwardly-pointing domains. This domain structure would be useful for the laser-heated poling experiments, since it would allow surface counter-poling from side laser heating to be seen regardless of the depth into the fiber of the Curie isotherm. Cooling at the same rate that accomplished counter-poling in slab samples should generate even larger temperature gradients in the smaller fibers. However, there was no reversal observed in fibers which were heat treated in the same way which produced reversal in slabs.

The slab work also suggested another electrode-less method of uniformly poling fibers. If a fiber could be somehow "built into" the surface of a slab, heat stored in the center of the slab should produce a temperature gradient across the fiber during cooling which might be sufficient to pole the fiber. Our first experiment along these lines consisted

of a fiber simply sitting on the surface of a slab and the use of rapid cooling starting below the Curie temperature, as in the slab experiments. No domain structure change was observed in the fiber, comparing the parts of the fiber touching the slab and those hanging off the edge of the slab in free air. Poor thermal contact could account for the negative result.

The above fiber results make it seem that the domain structure is somehow "frozen into" the as-grown fibers more strongly than in our slab samples. Several further experiments are indicated, including raising fibers clearly above the Curie temperature before cooling, and applying controlled thermal gradients within the furnace. A closer look at poling during growth using asymmetric heating is warranted. Any technique involving temperature gradients is preferable to electrical poling, since no electrode metallization has been discovered that will not diffuse into the sample at the required poling temperature.

3. Vapor transport equilibration

Vapor transport equilibration (VTE) has been suggested as a means of improving the homogeneity of $LiNbO_3$ fibers. We have concluded that control of stoichiometry is crucial in obtaining reproducible results in cladding and poling experiments, as well as in determining the phasematching temperature. For our first fiber device demonstrations, we have decided that maintaining the congruent composition is most desirable. The most interesting results to report here, however, are on the use of VTE to produce material in which the Li/Nb ratio is equal to unity, a composition which cannot be grown directly using conventional crystal growth techniques. Fibers of this composition might be used in the future to generate shorter wavelengths than are currently achievable in congruent $LiNbO_3$.

In the VTE process, the samples are enclosed in a platinum crucible filled with lithium-rich powder (a mixture of $LiNbO_3$ and Li_3NbO_4 powders). They remain in this lithium-rich environment at 1100°C for a time long enough to ensure a homogeneous lithium content inside the material. The composition of the crystal after this treatment is truly stoichiometric. The diameter of our single crystal fibers is on the order of tens of microns and this gives a required equilibration time of only a few hours. A patent on the nonlinear optical applications of material which can be produced using this process has been filed.

The excellent homogeneity of the stoichiometric material produced by VTE is demonstrated in Fig. 4. The width of the temperature phasematching curves is theoretically inversely proportional to the length of the nonlinear crystal for perfectly homogeneous material. The experimentally obtained tuning curves in Fig. 4 not only closely approximate the theoretical $sinc^2$ shape, but display widths which scale in inverse proportion to the sample lengths.

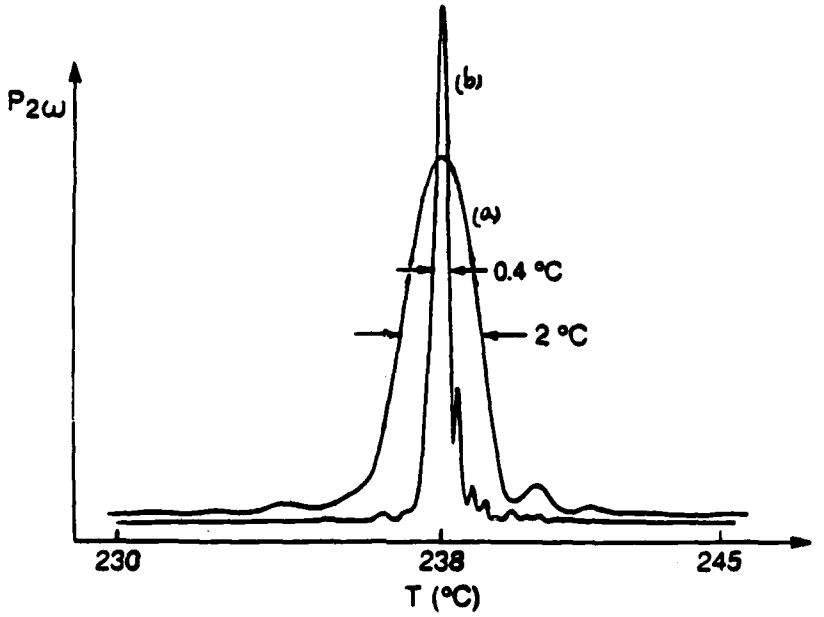

Fig. 4. Second harmonic generation temperature tuning curves for stoichiometric $LiNbO_3$ produced by vapor transport equilibration (see text). Curve (**a**): sample 4 mm long; curve (**b**): sample 20 mm long. Note that the widths of these curves are inversely proportional to sample length, indicating excellent composition homogeneity.

The optical properties of this new composition are different from those of the starting material. The birefringence is increased, which raises the phasematching temperature for a given wavelength (note that in Fig. 4, the phasematching temperature has been raised from 4°C for congruent material to 238°C for this stoichiometric material). Equivalently, the increased birefringence allows frequency doubling at shorter wavelengths. We have demonstrated that radiation at the wavelength 954 nm noncritically phasematches at –37°C to produce 477-nm light. This is the shortest wavelength ever produced in a bulk interaction in lithium niobate.

To design nonlinear devices such as frequency doublers and optical parametric oscillators, it is crucial to know the wavelength dispersion and temperature dependence of the refractive indices. We performed refractive index measurements on a prism cut from an equilibrated 1-mm thick wafer. The temperature dependence was measured by counting interference fringes from a thin sample as it was heated up to 150°C. From this data, a temperature-dependent Sellmeier fit could be deduced. To check the accuracy of this fit, we measured the tuning curve of the parametric fluorescence at three different pump wavelengths. This data is compared to the theoretical fit in Fig. 5. The agreement is good except for an offset of about 10 degrees at higher temperatures. In Fig. 6, measured noncritical phasematching temperatures for frequency doubling are compared to the fit data. Here, the discrepancy is larger. We are working on refining the Sellmeier fit to get more accurate predictions for phasematching temperatures. A manuscript is being prepared for publication which will report these measurements. Knowledge of the changes in the Sellmeier coefficients upon going to the stoichiometric composition may help us predict the refractive indices and their variation with temperature at different intermediate compositions.

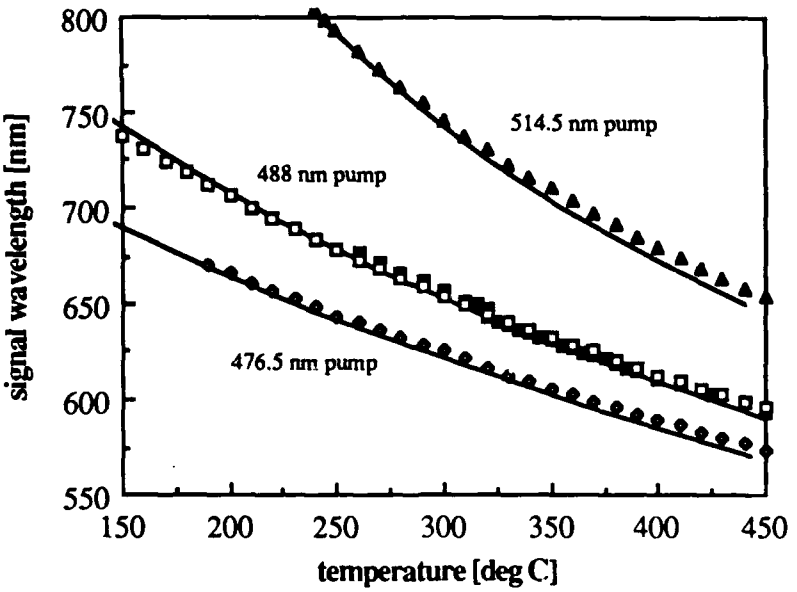

Fig. 5. Measured tuning curves of parametric fluorescence in stoichiometric $LiNbO_3$ (points) compared to theoretical Sellmeier fits (curves) obtained from independent refractive index measurements.

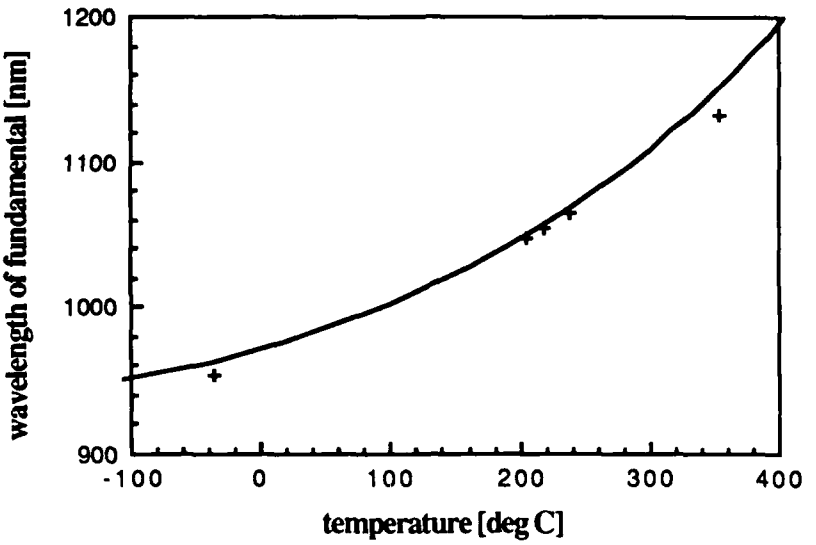

Fig. 6. Measured noncritical phasematching temperatures for frequency doubling of various wavelengths (crosses) compared to temperatures predicted from Sellmeier fit (curve).

For the congruent Li/Nb ratio, there is a maximum in a plot of phasematching temperature vs Mg doping concentration. There is likewise a maximum phasematching temperature for material in which the magnesium concentration is held at 5% but for which the Li/Nb ratio is varied. These two experimental facts suggest that a composition can be found within the Li_2O-Nb_2O_5-MgO system which is still a Mg-doped $LiNbO_3$ phase, but which possesses an even higher birefringence than pure stoichiometric $LiNbO_3$. Judging from Fig. 6, only a slightly higher birefringence may be needed to phasematch for doubling the 946 nm Nd:YAG line at close to room temperature. We are beginning a more detailed study of the Li_2O-Nb_2O_5-MgO pseudo-ternary phase diagram in order to address some of these issues, as well as to understand the kinetics of Mg diffusion into $LiNbO_3$ for the cladding work.

4. Cladding of $LiNbO_3$ fibers

Our initial experiments on the diffusion of magnesium into $LiNbO_3$ fibers have given us estimates of the change of refractive index with magnesium concentration and confirmed the diffusion coefficient of 3.6 $\mu m^2\ h^{-1}$ at 1050°C measured by Noda *et al.* [J. Appl. Phys. **49**, 3151 (1978)]. Magnesium concentration profiles were determined by

electron microprobe, and refractive index profiles were measured using a special magnifying Mach-Zehnder interferometer.

These first experiments produced a 3-mm long, 56-μm diameter *c*-axis fiber with a clad parabolic index profile. This fiber supported two guided modes at 633 nm. The fundamental mode diameter was estimated at 14 μm from far-field measurements of beam divergence and Gaussian beam propagation theory, a value consistent with the fundamental mode diameter calculated using the theory of mode propagation in a parabolic index profile. The refractive index profile and corresponding magnesium concentration profile measured for this fiber are shown in Fig. 7. A surface layer a few microns thick with a Mg/(Mg+Nb) ratio of about 7.3 at.% can be seen. This layer of roughly constant Mg concentration has possible applications as a step-profile cladding or a deep Mg diffusion source.

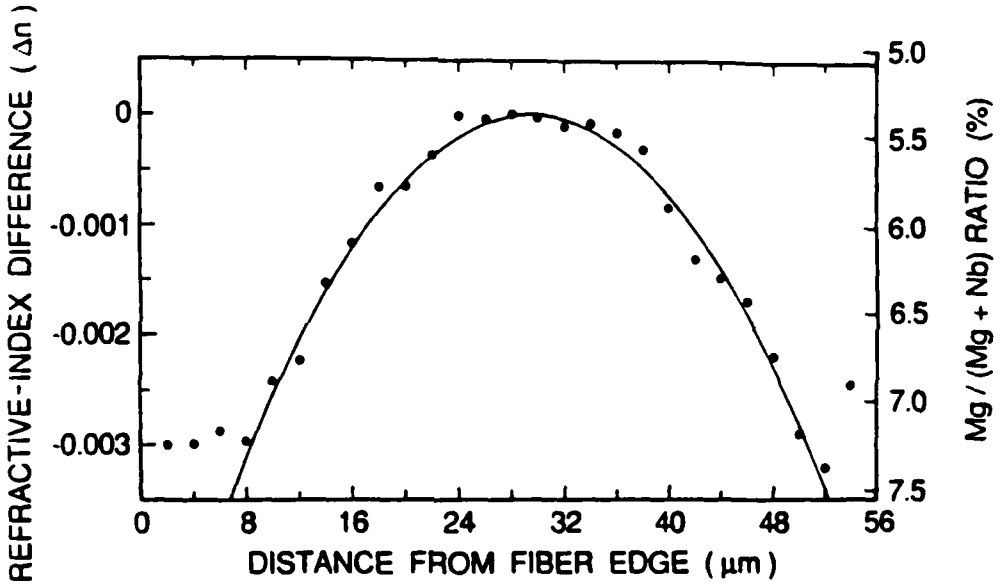

Fig. 7. Refractive index profile and measured Mg concentration plotted vs position across the *c*-axis, 56 μm, MgO:$LiNbO_3$ fiber used in the mode propagation experiment described in the text. Solid curve is best-fit parabola to center part of the profile.

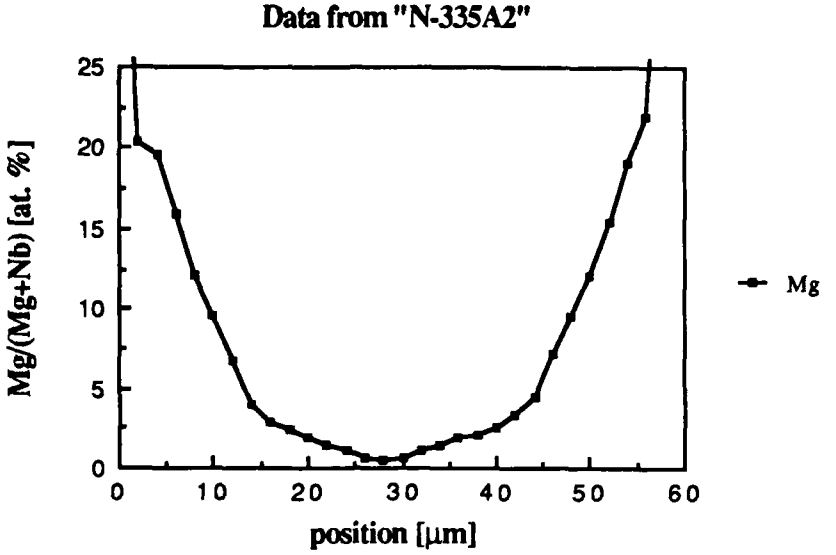

Fig. 8. Magnesium concentration as measured by electron microprobe vs position across an undoped congruent $LiNbO_3$ fiber. Note "kinks" at around 4 at. %.

The mode-guiding properties of this fiber have not yet been duplicated. In addition, random fluctuations of the depth of the Mg-rich surface layer and fiber breakage problems presumably caused by this layer suggested that fiber stoichiometry control at the congruent Li/Nb ratio composition would be helpful. (The solubility of Mg is believed to be greater at this composition than at the higher Li concentrations used in the first experiments, discouraging what is believed to be precipitation of the surface layer.) Magnesium-oxide doped "congruent" $LiNbO_3$ also has a convenient phasematching temperature for frequency doubling 1.06 μm radiation.

Our first diffusions into undoped congruent fibers in controlled congruent atmospheres suggested a concentration-dependent Mg diffusion coefficient. Note, for example, the change in slope of the diffusion profile shown in Fig. 8 at a magnesium concentration of around 4 at. %. In order to separate geometrical effects from true concentration-dependent diffusion effects, a series of diffusion experiments into slabs has been initiated. Finite source diffusions indicated a linear diffusion coefficient with the same coefficient as measured before, but the integrated profile did not contain all of the Mg which was deposited. Experiments in slabs with a 5% Mg starting concentration were then conducted to determine the behavior at higher Mg concentration, a condition which will exist near the surface during at least the early part of any diffusion. Careful study of the

diffused surfaces revealed the formation of a compound containing ~ 32 at. % Mg, which subsequently flaked off of undoped substrates. This observation explains the missing magnesium in earlier experiments. Data from slab experiments indicate a Mg diffusion coefficient which is independent of concentration up to the point at which the 32% compound forms. Anomalies in fiber diffusion profiles thus may well be due to geometry. Experiments in Mg-doped fibers are underway to determine this. Once a reliable picture of the Mg diffusion process is obtained, diffusion profiles in the fiber geometry can be predicted, and the refractive index profiles can be optimized for waveguiding.

5. Fiber handling

Alignment fixtures and procedures for mounting seed and source rods in capillary tubes for fiber growth were developed. Seeds and source rods mounted parallel to the capillary tube axis, which determines the direction of translation, are especially important in the growth of small-diameter fibers, because of the problem of gradually walking out of the focal spot of the heating laser. Ultraviolet-cured epoxy was found to be very useful for "tacking" the fibers in position before applying the high-temperature cement, which otherwise would pull them out of alignment because of its shrinkage during curing. UV epoxy was also found to be convenient for mounting fibers to the small capillary tubes used as handles during the deposition of MgO prior to cladding diffusions. Breakage problems during the handling and mounting of small fibers have been greatly reduced by the development of special vacuum pickup tips and v-groove chucks which are used with a commercial vacuum parts-handling wand.

6. Fiber characterization

As mentioned in the cladding section, an interferometric technique has been used in the measurement of refractive index changes due to Mg in-diffusion. A standard Mach-Zehnder interferometer has been set up with a HeNe laser source. In the sample arm, a microscope objective forms a magnified image of the sample (a flat polished cross-section of a fiber less than a millimeter thick) at the combining beamsplitter. A matching microscope objective is placed in the reference arm an equivalent distance from the output beamsplitter. An interference pattern between the two overlapping spherically diverging waves forms at the beam combiner. The mirror tilts and path lengths are adjusted to give closely-spaced, almost-parallel fringes across the fiber image. The fiber cross-section with

superimposed interference pattern is further magnified by another objective, which forms a real image on a screen or photographic film.

The first second harmonic generation experiments in clad 50-μm fibers have been performed. In the most recent experiment, an undoped congruent fiber with transverse dimensions 45 x 57 μm was used. The *a* axis was along the fiber, whose length was 9.6 mm. The fiber had an as-grown domain structure (one domain wall lengthwise along the fiber), and a diameter uniformity of several percent (it was grown open-loop). It was clad by an unoptimized MgO in-diffusion.

The measured second harmonic generation efficiency was much less than what one would expect from an optimally-focused bulk interaction in a large crystal of the same length. The ugly output "mode" speckle-pattern and the fact that the best conversion was obtained at 140°C instead of 4°C expected for an all-fundamental mode interaction made it obvious that this was an interaction between high-order modes with poor overlap, with a small fraction of the fundamental wavelength power actually phasematched. We conclude that efficiency is currently limited by modal scattering. With the achievement of good mode propagation we can expect about a 50-fold enhancement of the conversion efficiency over a bulk interaction. This result clearly indicates that better waveguiding is the key to high efficiency frequency doubling — hence our current particular emphasis on cladding diffusion characterization. These results and an overview of the processing steps that go into making a fiber frequency doubler were presented at the OSA Annual Meeting in Rochester, NY in October.

7. Waveguide theory

The theoretical work on the mode properties and losses in birefringent fibers with arbitrary orientation has been extended. The theory has now been generalized to apply also to planar waveguides and graded structures with arbitrary anisotropy. A manuscript to be submitted for publication is now being revised to reflect these additions.

B. Second Harmonic Generation in DC-Biased Quantum Wells

Electrons in the conduction band of a quantum well are quantized in the direction normal to the layers into a series of eigenstates resembling those of "particles in a box." Transitions between intersubbands have large dipole matrix elements (oscillator strength or

the order of m_e/m^*, or 15 for GaAs) and tunable energy differences typically resonant with 5 – 15 μm radiation. These large matrix elements and resonant enhancements lead one to expect large nonlinear susceptibilities. Since square quantum wells are inversion symmetric, their second-order nonlinearity ($d^{2\omega}$) vanishes and enhancement occurs only in the third nonlinear susceptibilities. Under DC bias, this symmetry is broken (Fig. 9), and a large second-order susceptibility can be expected. While such a large susceptibility is interesting in its own right, the spatial and temporal modulation of the nonlinearity by controlling the applied fields greatly enhances the utility of this phenomenon. For example, a periodic electrode structure with alternating positive and negative bias creates a sign grating in the $d^{2\omega}$ that can be used for quasiphasematching.

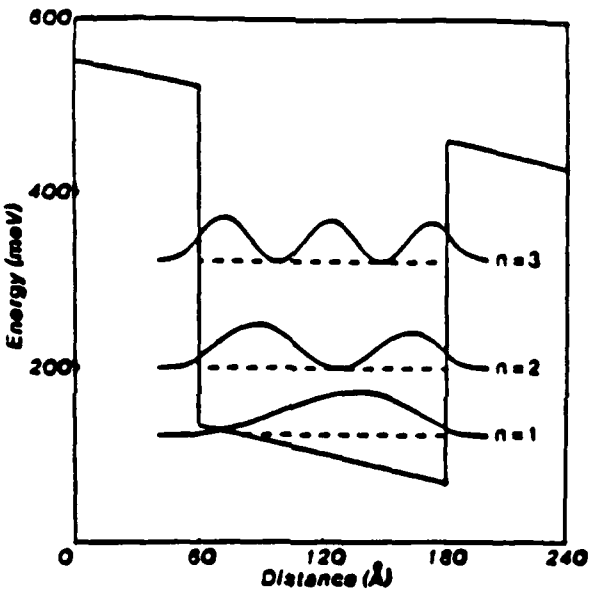

Fig. 9. The three bound states of a 120-Å GaAs quantum well between $Al_{0.5}Ga_{0.5}As$ barriers with an applied field of 50 kV/cm. Note the lack of inversion symmetry, particularly in the ground state.

Significant progress has been made toward the study of the second-order nonlinearity in the quantum wells since it started last year. Labs for characterizing the samples and for measuring their nonlinearity have been set up. We have succeeded in the first measurement of the quantum well $d^{2\omega}$, whose voltage dependence was in accordance with our theory.

1. Lab setup

A Digilab model FTS40 Fourier-transform infrared spectrometer has been installed and used intensively for characterizing intersubband states of the quantum well samples with a signal-to-noise ratio better than 10^5 (for an 8-second scan) and a resolution as high as 2 cm^{-1}. Using the sample held in a cryostat we obtained a number of spectra of the intersubband transition at various temperatures and voltages.

A carbon dioxide laser from Advanced Kinetics has been installed and successfully operated in both cw and Q-switched mode. A microrefrigerator from MMR is also installed to cool the sample down to liquid nitrogen temperature. Various electronic equipment is installed to bias the sample for a short duration in sync with Q-switch pulses and to average the detected second harmonic fluence.

2. Experiments

In the first part of the experiment, we monitored the voltage dependence of the second harmonic generation at various polarizations. Second harmonic waves are generated by both the quantum wells and the bulk substrate. The two fields add coherently and the total second harmonic fluence would be $I^{2\omega} = \left| d_{QW}^{2\omega} + d_{GaAs}^{2\omega} \cos\gamma \right|^2$, where γ is the polarization angle (constants have been omitted for simplicity). Since $d_{QW}^{2\omega}$ is proportional to the applied voltage, a plot of $I^{2\omega}$ vs voltage should look like a parabola whose center position is proportional to $\cos\gamma$. The experimental data shown in Fig. 10 proves our point clearly and is in good agreement with our theory.

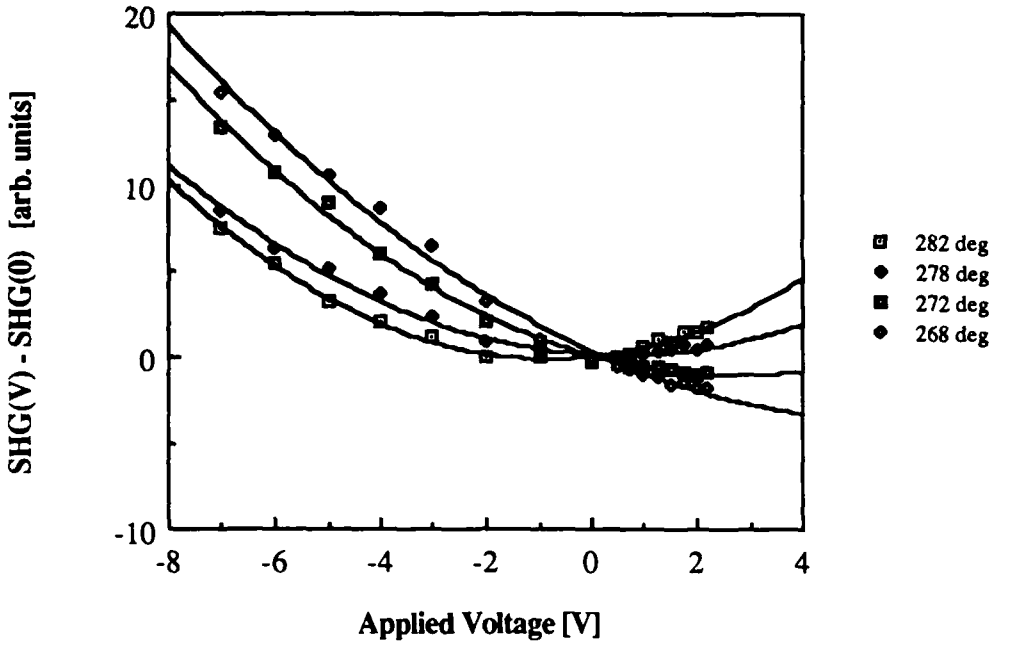

Fig. 10. Measured second harmonic fluence vs. applied voltage at various polarization angles. Vertical axis is the difference in the second harmonic fluence when voltage is applied and not applied. Polarization angle is shown on the right: 270° is the angle at which polarizers are aligned for Brewster's angle.

The second part of the experiment is to study the dispersion characteristics of $d_{QW}^{2\omega}$. By using a 108-μm thick bulk GaAs sample, we calibrated the measured $d_{QW}^{2\omega}$ at various wavelengths of the carbon dioxide laser (shown as triangles in Fig. 11). The measured $d_{QW}^{2\omega}$ is as large as 6×10^{-8} m/V (300 times larger than that of bulk GaAs), **the largest $d^{2\omega}$ reported for any material**. Shown in the same plot are the theoretical calculations of $d_{QW}^{2\omega}$ vs fundamental energy for different frequencies of the forbidden transition (n = 1 to 3). Notice here that $d_{QW}^{2\omega}$ is very sensitive to the precise location of the forbidden transition. We are refining our absorption measurements in an attempt to observe the almost-forbidden transition when the symmetry is broken by an applied field.

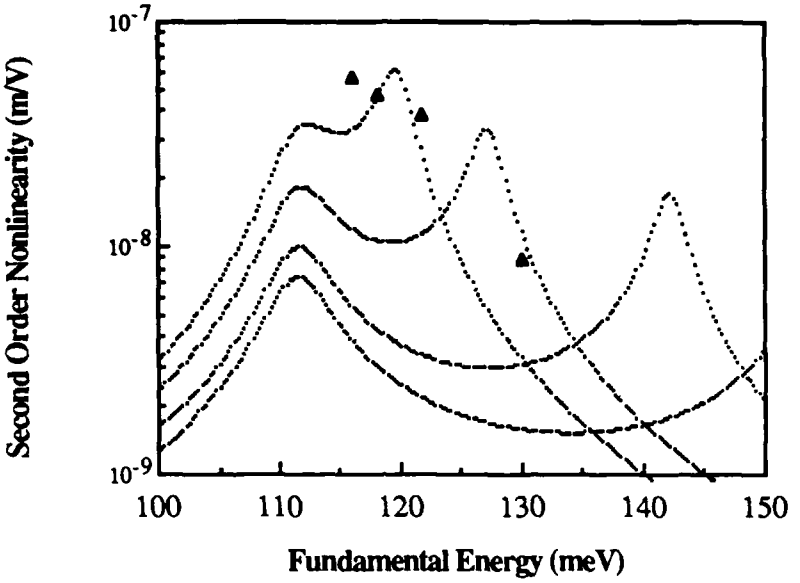

Fig. 11. Theoretical calculation of $d^{2\omega}$ vs fundamental energy for 92-Å GaAs well with 320-Å barriers, under an applied bias field of 36 kV/cm. Each curve assumes that the n = 1 to 3 forbidden transition is at a different frequency. Points are experimentally measured values.

3. Theoretical modeling

The theoretical model for second-order susceptibilities of subband transitions in biased square wells is essentially complete, and is being prepared for publication. Numerical calculations of the nonlinear susceptibility based on this model are shown in Fig. 11. The next theoretical topics we will study are the design of nonsquare potentials optimized for higher polarizability, control of the eigenspectrum to produce multiply resonant nonlinear interactions, the importance of intersubband dispersion for phasematching, and device optimization in the presence of background absorption.

4. Fabrication and processing

Another major thrust of the present work is to incorporate quantum wells in an optical waveguide. This step is important because the conversion efficiency is expected to increase by orders of magnitude from the confinement of the beam and the larger coupling

to the intersubband. Periodic bias electrodes can be fabricated on the top of the waveguide to create a periodic variation in the sign of the nonlinear coefficient. Such a structure will have obvious application to the quasiphasematching of arbitrary interactions. Chemical etching provides a convenient way of creating a strip load and grating couplers on a waveguide. Some grating couplers have been fabricated on Si and GaAs wafers (see Fig. 12) and the fabrication of an asymmetric grating for larger coupling efficiency is under investigation. The samples used in our studies were grown by J. S. Harris's group in the Stanford Electronics Laboratory. We will continue the collaboration with this group in the future.

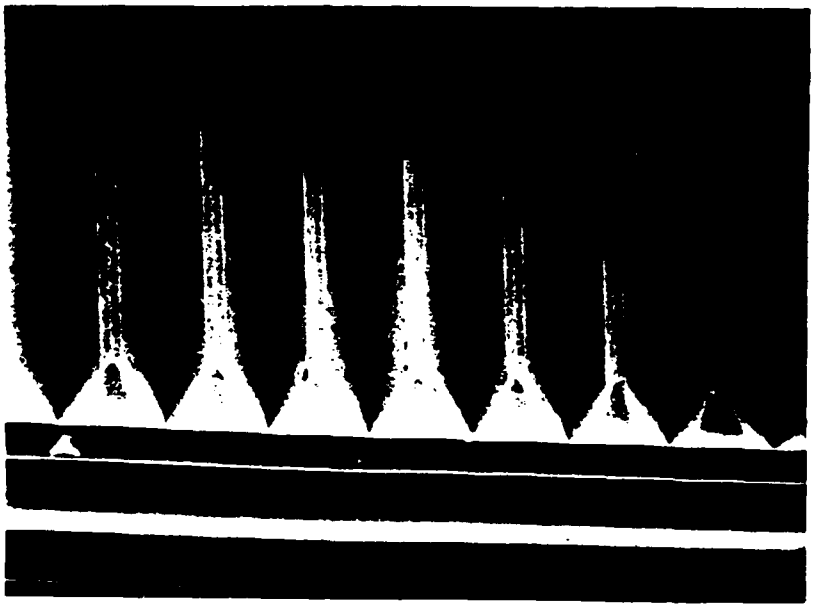

Fig. 12. Grating with 8-μm period fabricated on a ⟨100⟩ silicon wafer. The anisotropic nature of the chemical etchant produces V-shaped grooves.

C. Structural and Optical Studies of Thin Polysilane Films

The new class of organo-silane polymers consist of a long (>1000 atoms) backbone of σ-bonded silicon atoms with two organic substituent groups attached to each Si atom. These materials volatilize upon exposure to ultraviolet light, making them an efficient self-developing lithography material and have therefore been extensively investigated in the earlier part of the decade as photoresists. They have also been investigated as possible photoconductors, and as precursors to silicon carbide formation.

Attention has recently turned to investigation of the nonlinear optical properties of these materials. These properties should be analogous to the extensively studied carbon-based polydiacetylene polymer system, with the delocalized electrons arising from *d*-electron contributions to the outer orbital, rather than from conjugated π-bonds. Polysilanes, however, have several advantages as nonlinear materials. First, because of the interest in these materials as photoresists, the capability of fabricating thin (≤ 4 μm) films of excellent quality has already been developed. Second, the $\sigma \rightarrow \sigma^*$ absorption edge is typically ≈ 3.9 eV, so the material is transparent at all visible wavelengths. Finally, this absorption band edge is related to the unperturbed length of the silicon backbone, and can be shifted by adding various substituent groups to the silicon backbone, making resonant enhancement of various nonlinear effects at particular wavelengths possible.

Of special interest for nonlinear optical applications is the compound poly(di-*n*-hexylsilane), a polymer with two hexyl chains attached to each Si atom. At temperatures below 42°C, the hexane side chains undergo a crystallization which forces the Si backbone (normally helical) into a planar zigzag conformation. This crystallization occurs only on a microscopic scale; no evidence of spontaneous macroscopic orientation has been observed for this compound. The higher dipole moment associated with this new orientation can be seen in the formation of a strong absorption shifted from 313 nm (the peak for the amorphous region) to 375 nm, and also in a dramatic increase in the $\chi^{(3)}$ nonlinearity. Third harmonic generation measurements by Baumert *et al.* at IBM have shown this may be as large as an order of magnitude as the material goes through this phase transition. They report a value of $\chi^{(3)}(-3\omega; \omega,\omega,\omega) = 11.2 \times 10^{-12}$ esu (at $\lambda = 1.06$ μm) for the crystalline phase.

We have begun the investigation of optical nonlinearities of polysilanes, and in particular, poly(di-*n*-hexylsilane) in this laboratory. Films up to 4 μm thick have been made available by arrangement with Robert D. Miller and C. Grant Willson of the IBM Almaden Research Center. The original intent of the research has been twofold: first, to measure various nonlinear processes of the material, and secondly, to fabricate and study waveguide devices which can exploit some of these nonlinear processes.

The first experiment carried out in this lab was an attempt to measure $\chi^{(3)}(-\omega; \omega,\omega,-\omega)$ with a simple four-wave-mixing experiment using a pulsed dye laser. This experiment was unsuccessful, however, because it was discovered that exposures to high laser intensities (> 1 MW/cm^2) at 560 nm needed for observation of nonlinear effects induced permanent photochemical changes in the material. These changes appeared as a

marked birefringence (as high as $\Delta n = 0.03$) in the thin film, oriented along the exposing laser polarization. Large changes in the UV absorption spectrum also accompany these index changes. Because the index change can be varied with dose, it should be possible to use this effect to fabricate channel waveguides by photoexposure.

This effect has been studied in more detail by comparing the absorption spectra of films exposed to doses of directly absorbed UV light to the changes caused by exposure to high-intensity 560-nm light. A plot of a typical absorption spectrum of a 700-nm thick film of poly(di-*n*-hexylsilane) after various doses of exposure to a polarized 0.3 mW cw HeCd laser at 325 nm is seen in Fig. 13. For small exposures, the absorption peak shifts to shorter wavelengths, indicating destruction of the longer polymer chains. For longer exposures, the entire absorption is bleached and the photoproducts evaporate, leaving pronounced surface depressions in the film. Different behavior is observed when the films are exposed to high intensities of lower energy photons. In Fig. 14, the effect of exposure to polarized, pulsed 560-nm dye laser light at an intensity of 12.5 MW/cm^2 is shown. A similar absorption shift is seen, but only for light polarized parallel to the polarization of the original exposing laser light. No large surface changes were observed below the damage threshold of the material ($\approx$ 30 MW/cm^2).

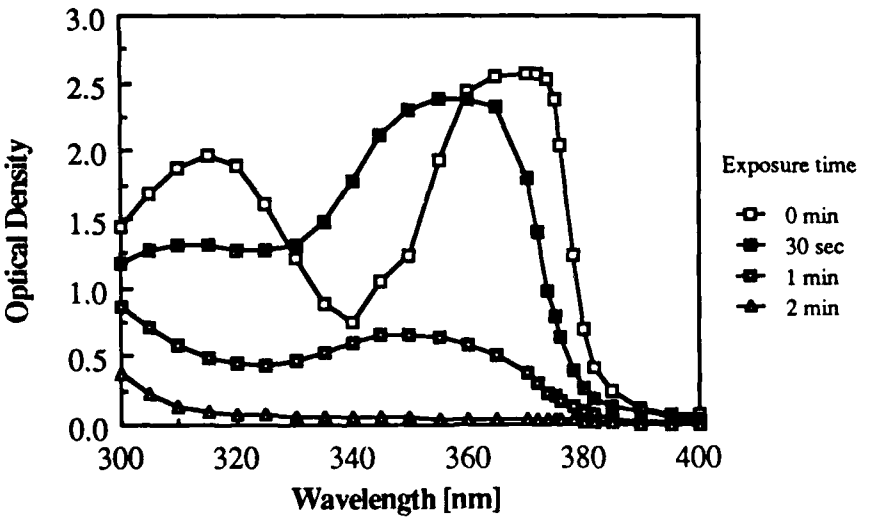

Fig. 13. Bleaching of polysilane film from exposure to 300 μW of cw 325-nm laser light.

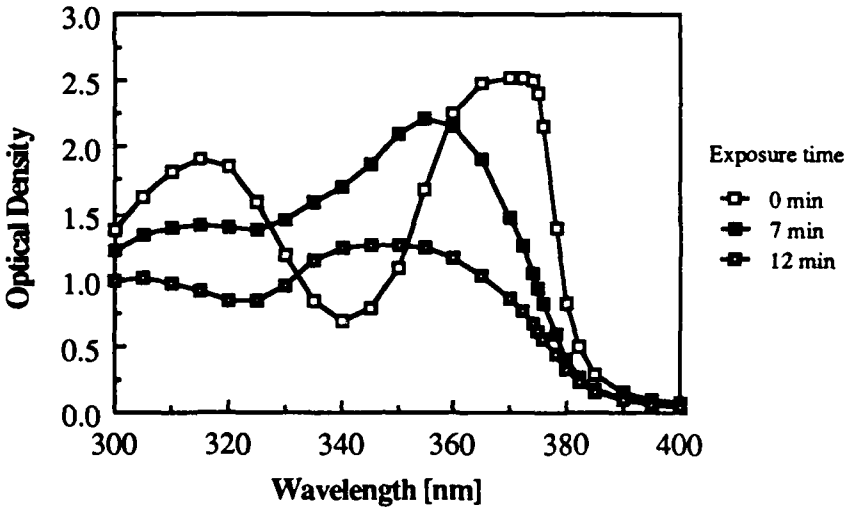

Fig. 14. Bleaching of polysilane film from exposure to 34 mW of pulsed 560 nm light.

More revealing than these absorption spectra are plots of the change in absorption, as shown in Fig. 15. In this case, it is clear that small exposures cause a marked change in absorption at 375 nm, indicating the destruction of the longest chain segments. This is accompanied by an marked increase in absorption at 340 nm, presumably due to the photoproducts of the reaction. A plot of the change in absorption of the 375-nm absorption feature for constant exposure dose of 13.4 J as a function of laser intensity is shown in Fig. 16. The change in absorption is fit within experimental error by a parabola, suggesting a two-photon absorption process.

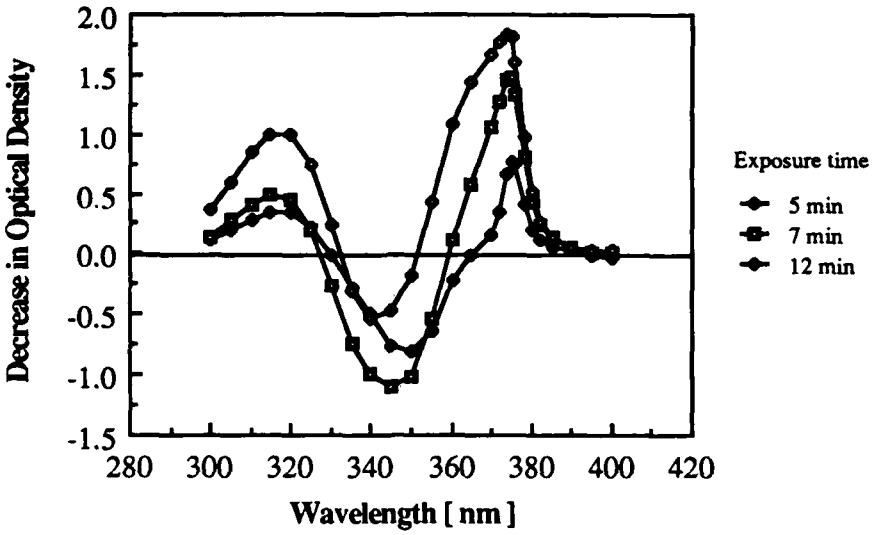

Fig. 15. Change in polysilane absorption spectrum at constant intensity for various doses of pulsed 560 nm light.

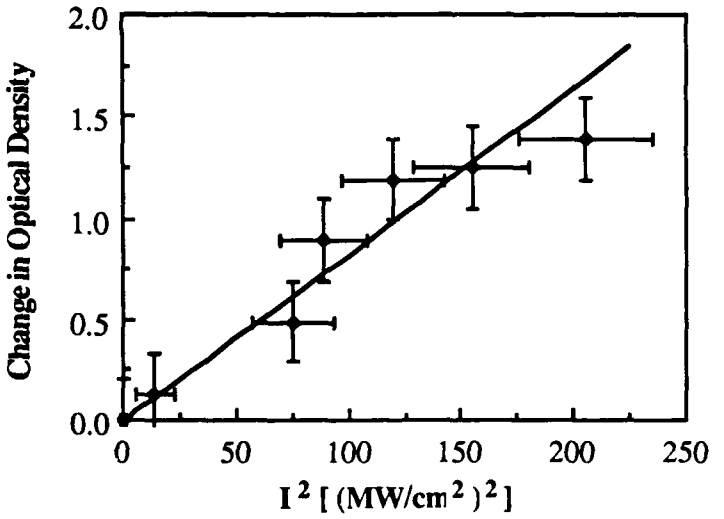

Fig. 16. Change in polysilane sample optical density at 375 nm for a 13.4 J exposure dose of 560-nm pulsed laser light. Fit is $\Delta(OD) = 8.2 \times 10^{-3} I^2$, where the intensity I is given in MW/cm^2.

This quadratic dependence is independent of film thickness or substrate material, indicating that bleaching is not related to thermal changes in the film. Further evidence for a two-photon process comes from a comparison of exposures at 532 nm and 1.06 μm with comparable doses of 560-nm dye laser light. Exposure at 532 nm induced a change in absorption which was smaller than that for 560 nm by about 30%, while no absorption change was observed for exposures at 1.06 μm. This is not unexpected. The linear absorption data indicate that, while $2h\nu$ for 560 nm corresponds to strong absorption of the amorphous band, $2h\nu$ for 532 nm corresponds to a gap in the energy levels of the medium and $2h\nu$ for 1.06 μm is well below the band edge.

Two-photon excitation at 560 nm falls in the same excitation band as absorption at 325 nm, so the mechanism of energy transfer and chain scission is expected to be similar. Consequently, it should be possible to interpret an approximate numerical value for $\chi^{(3)}$ governing the process by comparing the change in absorption for the one- and two-photon cases. An exposure of 13.4 J at 560 nm with intensities of 12.8 MW/cm^2 produces the same change in absorption of the 375 nm band as a cw exposure of 4.5 mJ at 325 nm. Using $\alpha_{325\ nm} = 52.6 \times 10^3\ cm^{-1}$, and assuming the absorbed energy transfer mechanisms are the same in both cases, we can calculate, following Shen's standard treatment in *The Principles of Nonlinear Optics* [Wiley, 1984],

$$\text{Im}\ \chi^{(3)}(-\omega;\ \omega,\omega,-\omega) \approx 3.2 \times 10^{-10}\ \text{esu}\ .$$

This value is five orders of magnitude larger than $\chi^{(3)}$ for fused silica, and is an order of magnitude lower than measured values for PTS polydiacetylene. Because the complex dynamics of energy transfer from the amorphous state (where the energy is absorbed) to the crystalline state (where the bonds are broken), as well as the intermediate steps in the multi-step chain scission process, are not clear at this time, this value can only be considered an estimate.

IV. PROPOSED FUTURE RESEARCH DIRECTIONS

The emphasis of our research program has obviously grown to incorporate studies on the modification of the properties of nonlinear media using a variety of techniques and structures. More complete and detailed suggestions for future work from this general perspective can be found in our latest AFOSR proposal, "Synthetic Nonlinear Media." What follows is an overview of our plans for the immediate future, as suggested by the results presented in this report.

A. Oxide Crystals

We are beginning work in the area of Nd-doped doped lithium niobate substrates. The intention is to investigate the possibility of constructing integrated optics devices that have gain. We have already demonstrated the diffusion of Nd^{3+} into an undoped $LiNbO_3$ substrate. This sample exhibits the same characteristic blue-green color as bulk crystals doped during Czochralski growth. More work is needed to determine the diffusion characteristics of Nd^{3+} in $LiNbO_3$ and the refractive index profile induced by the Nd doping profile.

In addition to our current experiments on $LiNbO_3$, we will also be conducting ferroelectric poling experiments on $LiTaO_3$ plates. Lithium tantalate has a lower Curie temperature than does lithium niobate. This may make it easier to accomplish periodic poling in lithium tantalate than in lithium niobate. If we can perform periodic poling in lithium tantalate, we will be able to take advantage of its its lower tendency to photorefractively damage, and its d_{33} coefficient, which is larger than the commonly used d_{15} coefficient of lithium niobate.

We have begun studies on the growth of $LiTa_xNb_{1-x}O_3$ mixed-crystal fibers. The compounds $LiNbO_3$ and $LiTaO_3$ can coexist in a solid solution over the entire range of x values. Lithium tantalate has a slight positive birefringence, whereas lithium niobate is negatively birefringent. It is possible to produce a mixed crystal with any birefringence in between for phasematching purposes — even a crystal with zero birefringence, if so desired. Preliminary microprobe data on a mixed-crystal fiber indicate a higher Ta concentration toward the outside edge of the fiber, which, since the Ta-rich material has a

lower refractive index than the Nb-rich material, raises the intriguing possibility of a "self-clad" mixed-crystal fiber.

Work on the phase diagram of the Li_2O-Nb_2O_5-MgO system has been initiated. Knowledge of the details of this phase diagram will be helpful in understanding the Mg diffusion cladding process, and, perhaps more importantly, lead to the engineering of $LiNbO_3$ material with tailored phasematching temperatures. Lithium niobate may even prove to be useful for the generation of blue wavelengths through noncritically-phasematched frequency doubling of the 946-nm line of miniature Nd:YAG lasers.

B. SHG in DC-Biased Quantum Wells

The results we obtained from the quantum well experiments are very encouraging. The measured large $d^{2\omega}$ and the controllability of its sign promise efficient second harmonic generation in a waveguide structure. Our immediate future effort will be focused on further study of the $d^{2\omega}$ of intersubband transitions and the modeling of waveguide structures.

By tailoring design parameters such as the shape of the wells and the magnitude and distribution of the donor density, one can increase $d^{2\omega}$ while decreasing the absorption coefficient. For example, biased square wells have larger $d^{2\omega}$ when the second harmonic is resonant with the forbidden transition than when the fundamental is resonant with the allowed transition. The total linear absorption, however, will be at least two orders of magnitude smaller when using the forbidden-transition resonance.

An understanding of tunneling and thermionic processes in the quantum wells is also important for reducing the current through the sample. By suppressing these two processes, we will attempt second harmonic generation at room temperature.

Epitaxial growth of AlGaAs permits the fabrication of waveguides with non-monotonic index profiles which can have interesting dispersion behavior. Modeling of waveguides optimized for efficient second harmonic generation will be an important task. Fabrication of grating couplers, strip loads and ohmic contacts on the waveguide will be pursued.

By the end of this year, we expect to complete the design and fabrication of a strip-loaded waveguide incorporating quantum wells and achieve efficient second harmonic generation through quasiphasematching.

C. Nonlinear Optical Properties of Polysilane Films

An encouragingly large estimate for the value of the third-order nonlinear susceptibility in a polysilane material has been obtained, but the dynamics of the photochemical and nonlinear optical processes occurring in polysilanes need to be investigated in more detail. Further measurements for this purpose include precise measurements of photoemission spectra of both the room-temperature and high-temperature phases for various doses of photoexposure. We also intend to make more measurements over a range of wavelengths using several different laser dyes to see the effect of excitation by two-photon absorption into both the crystalline and amorphous bands. Later in the year, once the effect has been characterized and exposure parameters established, we intend to use this material to fabricate integrated optical channel waveguides.

V. COLLABORATIONS

Sapphire fibers. Single-crystal sapphire fibers have a variety of potential applications. We have fulfilled the requests of several researchers for fiber samples to test for different purposes. For application to coal combustion diagnostics, we sent a fiber to P. Hansel (U.S. Dept. of Energy, Morgantown, WV). Fibers were sent to M. Bass (University of Southern California, Los Angeles, CA), W. Grundfest (Cedars-Sinai Medical Center, Los Angeles, CA), and H. Loertscher (Bascom Palmer Eye Institute, Miami, FL) for evaluation in a number of surgical applications involving the transmission of high-power laser light at the 3-μm wavelength and in the UV. We are collaborating with Brett Hooper, a University of Utah Laser Institute researcher working at the Stanford Photon Research Laboratory, to evaluate sapphire fibers for the transmission of 2–4 μm radiation from a free-electron laser for surgical applications. C.E. Byvik of NASA Langley Research Center (Hampton, VA) has used our fibers in studying the fluorescence and absorption properties of impurities in sapphire for use in space-based tunable laser systems. We have also provided sapphire fiber samples to S. DiVita of the U.S. Army Communication Electronics Command (Fort Monmouth, NJ), who is working the growth of GaAs on sapphire lightguides for integrated fiber-optoelectronic devices. The growth of sapphire fibers is now so well-understood that we have begun the transfer of the technology to LaserGenics, a San Jose-based startup firm that has licensed our implementation of the fiber growth process.

Other materials. Our collaboration continues with Prof. Robert S. Feigelson and his students at the Stanford Center for Materials Research, with emphasis on $LiNbO_3$ growth, poling, vapor transport equilibration, and phase diagram studies. We also collaborate with J. Nightingale and P. Bordui of Crystal Technology, Inc. on $LiNbO_3$ and $LiTaO_3$ materials studies and waveguide fabrication. We obtain III-V quantum well samples from Prof. J.S. Harris's group in the Stanford Electrical Engineering Department. L.C. West, presently of AT&T Bell Laboratories (Holmdel, NJ) was the first to observe direct intersubband transitions in such quantum well structures. We have had fruitful discussions with him regarding theoretical and experimental techniques for characterizing the quantum well material. Polysilane films for our studies of nonlinear optical properties have been provided by R. Miller's group at the IBM Almaden Research Laboratory.

VI. PUBLICATIONS, PRESENTATIONS, AND PATENTS

This list covers the full period of the contract. Publications, etc., which occurred during the final year are marked with an asterisk (*).

A. Publications

1. M.J.F. Digonnet, M.M. Fejer, and R.L. Byer, "Characterization of Proton-Exchanged Waveguides in MgO:$LiNbO_3$," Opt. Lett. **10**, 235 (1985).

2. M.M. Fejer, G.A. Magel, and R.L. Byer, "High-speed high-resolution fiber diameter variation measurement system," Appl. Opt. **24**, 2362 (1985).

3. John L. Nightingale, The Growth and Applications of Single-Crystal Fibers, Ph.D. Dissertation, Stanford University, September, 1985.

4. M.M. Fejer, J.L. Nightingale, G.A. Magel, W.J. Kozlovsky, T.Y. Fan, and R.L. Byer, "Nonlinear Optics in Single-Crystal Fibers," in *Tunable Solid-State Lasers for Remote Sensing*, R.L. Byer, E.K. Gustafson, and R. Trebino, eds., Springer-Verlag, Berlin, 1985, pp. 141–145.

5. M. Fejer, J. Nightingale, G. Magel, and R. Byer, "Single-Crystal Fiber Applications Include Nonlinear Effects," Laser Focus **21**, 60 (1985).

6. J.L. Nightingale and R.L. Byer, A Guided Wave Monolithic Resonator Ruby Fiber Laser," Opt. Comm. **56**, 41 (1985).

7. M.M. Fejer, M.J.F. Digonnet, and R.L. Byer, "Generation of 22 mW of 532-nm radiation by frequency doubling in Ti:MgOLiNbO$_3$ waveguides," Opt. Lett. **11**, 230 (1986).

8. Y.S. Luh, R.S. Feigelson, M.M. Fejer, and R.L. Byer, "Ferroelectric Domain Structures in $LiNbO_3$ Single-Crystal Fibers," J. Crystal Growth **78**, 135 (1986).

9. J.L. Nightingale and R.L. Byer, "Monolithic Nd:YAG Fiber Laser," Opt. Lett. **11**, 437 (1986).

10. Martin M. Fejer, Single-Crystal Fibers: Growth Dynamics and Nonlinear Optical Interactions, Ph.D. Dissertation, Stanford University, August, 1986.

11. G.A. Magel, D.H. Jundt, M.M. Fejer, and R.L. Byer, "Low-loss single-crystal sapphire optical fibers," *Infrared Optical Materials and Fibers IV*, Proc. SPIE **618**, 89 (1986).

*12. Y.S. Luh, M.M. Fejer, R.L. Byer, and R.S. Feigelson, "Stoichiometric $LiNbO_3$ Single-Crystal Fibers for Nonlinear Optical Applications," J. Crystal Growth **85**, 264 (1987).

*13. S. Sudo, A. Cordova-Plaza, R.L. Byer, and H.J. Shaw, "MgO:$LiNbO_3$ single-crystal fiber with magnesium-ion in-diffused cladding," Opt. Lett. **12**, 938 (1987).

*14. Amado Cordova-Plaza, $LiNbO_3$ Miniature Lasers and Single-Crystal Fibers, Ph.D. Dissertation, Stanford University, October, 1987.

*15. E.J. Lim, M.M. Fejer, G.A. Magel, Y.S. Luh, and R.L. Byer, "Ferroelectric domain reversal in $LiNbO_3$ plates due to the thermoelectric effect," to be submitted to Applied Physics Letters.

*16. M.M. Fejer, S.J.B. Yoo, Alex Harwit, R.L. Byer, and J.S. Harris, Jr., "Extremely Large Second-Order Susceptibility in AlGaAs Quantum Wells," manuscript in preparation.

*17. M. Lü, M.M. Fejer, and R.L. Byer, "Eigenvalues and modal fields of dielectric waveguides with arbitrary anisotropy," to be submitted to JOSA B.

B. Presentations

1. J.L. Nightingale and R.L. Byer, "Monolithic Resonator Single-Crystal Fiber Laser," paper WM36, presented by J.L. Nightingale at the Conference on Lasers and Electro-Optics, Baltimore, MD, May 21-24, 1985.

2. G.A. Magel, M.M. Fejer, J.L. Nightingale, and R.L. Byer, "Controlled Growth of Single-Crystal Optical Fibers," paper ThH2, presented by G.A. Magel at the Conference on Lasers and Electro-Optics, Baltimore, MD, May 21-24, 1985.

3. M.J.F. Digonnet, M.M. Fejer, and R.L. Byer, "Proton-Exchanged Waveguides in MgO:$LiNbO_3$," paper ThM45, presented by M.J.F. Digonnet at the Conference on Lasers and Electro-Optics, Baltimore, MD, May 21-24, 1985.

4. M.M. Fejer, M.J.F. Digonnet, and R.L. Byer, "Second Harmonic Generation in Ti:MgO:$LiNbO_3$ Waveguides," paper ThV1, presented by M.M. Fejer at the Conference on Lasers and Electro-Optics, Baltimore, MD, May 21-24, 1985.

5. M.M. Fejer and R.L. Byer, "Tailored Nonlinear Media," invited paper presented by M.M. Fejer at the Gordon Conference on Nonlinear Optics and Lasers, Wolfeboro, NH, July, 1985.

6. M.M. Fejer and R.L. Byer, "Growth and Applications of Single-Crystal Optical Fibers," invited paper WB2, presented by M.M. Fejer at the Optical Society of America Annual Meeting, Washington, DC, October 14-18, 1985.

7. G.A. Magel, D.H. Jundt, M.M. Fejer, and R.L. Byer, "Low-loss single-crystal sapphire optical fibers," paper 618-13, presented by G.A. Magel at Optoelectronic and Laser Applications in Science and Engineering (O-E/LASE '86), Los Angeles, CA, January 19-24, 1986.

8. J.L. Nightingale and R.L. Byer, "Monolithic Nd:YAG Fiber Laser," paper ThBB5, presented by J.L. Nightingale at the Conference on Integrated and Guided-Wave Optics, Atlanta, GA, February 26-28, 1986.

9. M.M. Fejer and R.L. Byer, "Nonlinear Interactions in Crystal Fibers," invited paper WR1, presented by M.M. Fejer at the Conference on Lasers and Electro-Optics, San Francisco, CA, June 9-13, 1986.

*10. Y.S. Luh, M.M. Fejer, R.S. Feigelson, and R.L. Byer, "Stoichiometric Lithium Niobate for Nonlinear Optical Applications," paper TuH2, presented by Y.S. Luh at the Conference on Lasers and Electro-Optics, Baltimore, MD, April 27 - May 1, 1987.

*11. Y.S. Luh, M.M. Fejer, R.L. Byer, and R.S. Feigelson, "Stoichiometric $LiNbO_3$ Single-Crystal Fibers for Nonlinear Optical Applications," presented by Y.S. Luh at the 7th American Conference on Crystal Growth, Monterey, CA, July 13-17, 1987.

*12. S.J.B. Yoo, M.M. Fejer, Alex Harwit, R.L. Byer, and J.S. Harris, Jr., "Second Harmonic Generation in DC-Biased Quantum Wells," paper MR10, presented by S.J.B. Yoo at the Optical Society of America Annual Meeting, Rochester, NY, October 18-23, 1987.

*13. G.A. Magel, S. Sudo, A. Cordova-Plaza, M.M. Fejer, H.J. Shaw, and R.L. Byer, "Second Harmonic Generation in Lithium Niobate Fibers," paper WR3, presented by G.A. Magel at the Optical Society of America Annual Meeting, Rochester, NY, October 18-23, 1987.

C. Patents

1. J.L. Nightingale, M.M. Fejer, and R.L. Byer, "Apparatus for translating crystal fibers," U.S. Patent No. 4,607,776, issued August 26, 1986.

*2. M.M. Fejer, G.A. Magel, and R.L. Byer, "Method and means for high-resolution measurement of fiber diameter," U.S. Patent No. 4,650,322, issued March 17, 1987.

*3. Y.S. Luh, M.M. Fejer, R.L. Byer, and R.S. Feigelson, "Tailored properties of lithium niobate for nonlinear optical applications by vapor transport equilibration," filed January, 1988.

*4. M.M. Fejer and R.L. Byer, "Nonlinear Optical Processes in Electric-Field-Biased Quantum Wells," filed October, 1987.

VII. PERSONNEL ASSOCIATED WITH THE PROGRAM

Robert L. Byer — Principal Investigator
Professor, Applied Physics

Robert C. Eckardt
Senior Research Associate, Ginzton Laboratory

Martin M. Fejer
Acting Assistant Professor, Applied Physics

Graduate Students, Byer Group:

Gregory A. Magel

Dieter H. Jundt

Eric J. Lim

Mei Lü

S. J. Ben Yoo

Franklin M. Schellenberg

Graduate Students, H. John Shaw Group (Applied Physics)

Amado Cordova-Plaza

Whu-Ming Young

Graduate Students, Robert S. Feigelson Group (Materials Science and Engineering)

Yih-Shyong Luh

Visiting Scholar

Shoichi Sudo — N.T.T. Ibaraki, Japan

Advanced degrees awarded:

John L. Nightingale, Ph.D., September, 1985.
Dissertation title: The Growth and Applications of Single-Crystal Fibers

Martin M. Fejer, Ph.D., August, 1986.
Dissertation title: Single-Crystal Fibers: Growth Dynamics and Nonlinear Optical Interactions

Amado Cordova-Plaza, Ph.D., October, 1987.
Dissertation title: $LiNbO_3$ Miniature Lasers and Single-Crystal Fibers